# Reconciling models and measurements of marsh vulnerability to sea level rise

Daniel J. Coleman[1], Mark Schuerch[2], Stijn Temmerman[3], Glenn Guntenspergen[4], Christopher G. Smith[5], Matthew L. Kirwan[1]

1. Virginia Institute of Marine Science 2. Lincoln Centre for Water and Planetary Health, School of Geography, University of Lincoln 3. Ecosystem Management research group, University of Antwerp, Belgium 4. U.S. Geological Survey, Patuxent Wildlife Research Center 5. U.S. Geological Survey, St. Petersburg Coastal and Marine Science Center

**Tidal marsh survival in the face of sea level rise (SLR) and declining sediment supply depends largely on the ability of marshes to build soil vertically. However, numerical models typically predict survival under rates of SLR that far exceed field-based measurements of vertical accretion. Here, we measure suspended sediment concentration (SSC), and vertical accretion in seven marshes along the U.S. Atlantic Coast and compile data from 70 additional marshes from around the world. While marsh accretion at local scales is highly variable and poorly predicted by models, we find that over continental scales, 70% of variability in marsh accretion rates can be explained by simple physical characteristics, namely SSC and spring tidal range (TR). Accretion rates for a given SSC and TR are highest in low marshes and are consistent with threshold sea level rise rates predicted by numerical models. We explain apparent discrepancies between models and measurements by showing that measured deficits between rates of accretion and SLR are not necessarily representative of marsh drowning. Together these results help bridge the gap between models and measurements, and reinforce the paradigm that sediment supply is the key determinant of wetland vulnerability at continental scales.**

Accelerating rates of sea level rise and declining sediment yields threaten coastal landforms and the ecosystems that inhabit them (Fitzgerald et al., 2009; Kirwan and Megonigal, 2013; Syvitski et al., 2009). Coastal wetland vulnerability is best characterized through spatially explicit metrics that incorporate lateral competition between erosion, progradation, and inland migration (Ganju et al., 2017; Kirwan et al., 2016; Mariotti, 2020), but at the most fundamental level, existing wetlands must build soil vertically faster than the rate of sea level rise to survive (Redfield, 1972; Reed, 1995; Friedrichs and Perry, 2001). Wetlands build soil elevation by trapping mineral sediment and accumulating organic matter, which are processes that tend to increase under accelerating rates of sea level rise (Kirwan and Megonigal, 2013). However, sediment delivery to the coast has significantly declined in many regions of the world (Wang et al., 2011; Weston 2014), meaning that wetlands are potentially receiving less inorganic material to build soils at ever faster rates. Indeed, observations of wetland loss today (Jankowski et al., 2017; Morris et al., 2016; Crosby et al. 2016) and in the stratigraphic record (Tornqvist et al., 2020; Saintalin et al., 2020) indicate that there are limits to wetland accretion that must be quantified to predict how valuable coastal ecosystems will respond to global change.

The maximum possible rate of vertical accretion defines a threshold for wetland survival, beyond which sea level rise leads to wetland drowning. However, estimates for threshold rates of SLR differ drastically, especially between projections from numerical simulation models and empirical measurements. Numerical models often predict stability under relatively high future rates of SLR (Kirwan et al., 2016; Scheurch et al. 2018), whereas contemporary field measurements suggest vulnerability at rates of SLR observed even today (Jankowski et al., 2017; Morris et al., 2016; Crosby et al. 2016). For example, a meta-analysis of vertical accretion rates suggests widespread (>66% of 98 sites) drowning at rates of SLR of 5 mm $yr^{-1}$ (Crosby et al., 2016), despite numerical models that predict marsh survival at SLR rates of up to 10–50 mm $yr^{-1}$ (Kirwan et al. 2016). Modeled threshold rates

48 depend strongly on sediment supply and tidal range (Kirwan et al. 2010), suggesting that discrepancies
49 between models and observations may partially be related to variability within and between marshes.
50 However, under conditions generally representative of U.S. Atlantic Coast estuaries (spring tidal
51 range=1 m; suspended sediment concentration=30 mg $L^{-1}$), measurements of organic and inorganic
52 contributions to soil accretion suggest drowning under SLR rates greater than ~5 mm $yr^{-1}$ (Morris et al.,
53 2016), while an ensemble of numerical models predicts a threshold SLR rate twice as high (Kirwan et
54 al., 2010).

55 There are inherent advantages and disadvantages to using both numerical models and empirical
56 measurements to predict the maximum rate of SLR that existing marshes can survive without having to
57 migrate landward. Numerical models typically focus on basic feedbacks between inundation and
58 sediment transport that allow projections of elevation building through time in response to changing
59 environmental conditions (Fagherazzi et al., 2012; Kirwan et al., 2016). Yet, models are inherent
60 simplifications of real-world process that often rely on basic treatment of vegetation, non-volumetric
61 sediment budgets, lack of spatial resolution, and sensitivity to poorly constrained parameters such as the
62 concentration and settling velocity of suspended sediment (Tornqvist et al., 2019; Wiberg et al., 2020).
63 Field measurements, on the other hand, directly measure current and historical rates of vertical accretion
64 influenced by a more complete suite of processes (DeLaune et al., 1978; Parkinson et al., 2017;
65 Jankowski et al. 2017). Accretion rates tend to increase with flooding depth and duration (Friedrichs and
66 Perry, 2001; Temmerman et al. 2003), making it difficult to project measurements based on current or
67 historical conditions into a future characterized by faster SLR rates (Kirwan et al., 2016). Sediment
68 records covering multiple millennia offer evidence of how wetlands responded to SLR rates faster than
69 present rates (Horton et al. 2018; Tornqvist et al., 2020; Saintilan et al. 2020), but it remains unknown

how other differences (e.g. atmospheric $CO_2$ concentrations) may have affected marsh response in the past.

Here, we attempt to bridge the gap between numerical models and field measurements by developing an empirical model of salt marsh vulnerability based on novel field measurements and a global meta-analysis of accretion and suspended sediment concentration (SSC). Our work finds that vertical accretion and marsh vulnerability are fundamentally tied to SSC and spring tidal range (TR), and suggests that perceived differences between models and measurements can be explained by the difference between marsh elevation loss relative to sea level and marsh drowning.

## Drivers of Vertical Accretion

We directly measured SSC and vertical accretion in seven tidal marshes spanning the eastern coast of the US and one on the eastern coast of Australia (Figure 1). In contrast to the traditional approach of quantifying SSC using bottle sampling and vacuum filtration (e.g. Christiansen et al., 2000; Leonard and Reed, 2002; Moskalski and Sommerfield, 2012; Poirier et al., 2017; Wang et al., 1993; Ensign et al. 2017a), we measured SSC via optical back-scatter sensors every 15 minutes over seasonal to annual time scales and on the marsh platform rather than relying on discontinuous or channel-based measurements. Four of these sites were located within extremely low elevation, youthful marshes, evidenced by recent expansion or recovery from disturbance (Figure 1B; See Supplementary Material). We selected low marshes as they are thought to have local maximum rates of vertical accretion because of a negative feedback between inundation, plant productivity, and sediment deposition (Morris et al., 2002; Mudd et al., 2010; Kirwan and Guntenspergen, 2012; Cadol et al., 2014; Kirwan et al., 2016). Therefore, maximum accretion rates measured in low marshes are considered here to represent the maximum SLR rates that marshes could keep up with by sediment accretion. To complement these

93 measurements, we compiled vertical accretion and SSC data from the literature for 70 additional tidal
94 marshes around the world, with the greatest concentration of sites in Europe and North America (Figure
95 1). In contrast to our direct field measurements, these sites varied widely in marsh elevation, tidal range,
96 vegetation type, and the methodology used to measure accretion and SSC (Supplementary Table 1).
97 Therefore, our analyses include marshes across a wide range of environmental gradients; SSC ranged
98 from approximately 5-30 mg $L^{-1}$ and TR from 1.1 to 3.6 m in low marsh monitored sites, whereas the
99 meta-analysis sites encompassed a wider variety of SSC (0.5-358 mg $L^{-1}$) and TR (0.3-12 m).
100 Using this larger set of tidal marshes, we found that accretion rate is significantly related to
101 SSC*TR (robust linear regression, $R^2$=0.73, p<0.001; Figure 2a). We determined a simple empirical
102 model to describe this relationship (See Supplementary Material), defined as,
103 $$Accretion = C_1 * SSC * TR \quad (1)$$
104 This equation is analogous to accretion rate (mm $yr^{-1}$) having a fixed proportional relationship ($C_1$ in
105 mm L $m^{-1}$ $mg^{-1}$ $yr^{-1}$) to the sediment suspended in flooding waters (mg $L^{-1}$) during a spring high tide (m).
106 We calculated $C_1$=0.2212 ± 0.008 (± s.e.) for all sites excluding 5 outliers (See Supplementary
107 Material), which can be subdivided between $C_1$=0.1624 ± 0.0134 for high marsh sites and $C_1$=0.2250 ±
108 0.0114 for low marsh sites. The higher value of $C_1$ for low marshes is consistent with observations that
109 frequently flooded marshes have higher rates of accretion (Morris et al., 2002; Mudd et al., 2010;
110 Kirwan and Guntenspergen, 2012; Cadol et al., 2014; Kirwan et al., 2016). Furthermore, $C_1$ calculated
111 for only the four low marsh sites that we directly measured is even larger, $C_1$=0.3535 ± 0.0587,
112 supporting our assumption that these extremely low marshes would have local maximum accretion rates.
113 Interestingly, we found no significant difference between modern sedimentation measurements
114 ($C_1$=0.2452 ± 0.009) and modern elevation change measurements ($C_1$=0.1980 ± 0.019), suggesting that
115 shallow subsidence did not play a major consistent role in the relationship between SSC*TR and

accretion over regional-continental gradients (Cahoon et al., 2006). Accretion rates derived from both short-term measurements and long-term radiochronology were linearly correlated with SSC*TR, though the slope from measurements that integrated over long time periods (decades-centuries) ($C_I$=0.1014 ± 0.008) was less than that observed using modern accretion measurements (Figure 2b). This difference could be attributed to either accretion rates that are accelerating in parallel with SLR (Kolker et al., 2010; Kirwan and Temmerman, 2009) and/or the long-term effect of compaction and organic matter decomposition that are not fully expressed in short-term measurements (Kearney et al., 2004; Bartholdy et al., 2010; Tornqvist et al., 2008; Breithaupt et al., 2018; Tornqvist et al. 2020).

Conceptual and numerical models often emphasize the role of mineral sediment supply in determining marsh vulnerability to SLR (Reed, 1995; Mudd et al., 2004; FitzGerald et al., 2008; Kirwan et al., 2010; Fagherazzi et al., 2015; Kirwan and Megonigal, 2013), though attempts to demonstrate this in the field have been inconsistent. For example, many field studies do not find a relationship between average SSC and marsh accretion rates within a single study site (see Palinkas and Engelhardt, 2018; Murphy and Voulgaris, 2006; Poirier et al., 2017; D'Alpaos and Marani, 2016; Duvall et al., 2017). Similarly, the relationship between TR and accretion rates has been shown to be inconsistent (Kirwan and Guntenspergen, 2010), with some studies finding a positive relationship (Harrison and Bloom, 1977; Stevenson et al., 1986), some suggesting a negative relationship (Chmura and Hung, 2004) and some finding no relationship at all (Cahoon et al., 2006; French, 2006). In contrast, robust linear regression with all 77 of our marsh sites indicates that over 70% of the variability in accretion is explained by terms that directly relate to inorganic accretion, i.e. SSC and TR ($R^2$=0.73, $p<0.001$; Figure 2a). We suggest that the definitive role of physical processes becomes apparent only by considering SSC and TR together, and at regional to global spatial scales that encompass wider gradients in SSC and TR. Together, our results demonstrate the primary importance of inorganic accretion and support

assumptions of numerical models that aim to predict accretion rates based largely on physical processes (see Mudd et al., 2004; Kirwan et al. 2016; Temmerman et al., 2003; Marani et al., 2007).

Nevertheless, our work also illustrates substantial variability in accretion rates that cannot be explained by physical factors such as SSC and TR alone. Our empirical model predicts accretion rates that are more than twice as high as measured rates in many locations. For example, the empirical model predicts that marshes in the German Wadden Sea (SSC=34 mg $L^{-1}$, TR=2 m; Schuerch et al., 2013) should have accretion rates of ~15 mm $yr^{-1}$, whereas measured rates are only 3.5 mm $yr^{-1}$ (Schuerch et al., 2012). As discussed in the next section, we attribute this type of discrepancy to variability in the sampling locations on the marsh platform, where low marshes and those close to channels have higher accretion rates than high elevation marshes far from channels (this study; Stoddart et al., 1989; Bricker-Urso et al., 1989; Friedrichs and Perry, 2001; Temmerman et al., 2003). Variability in predicted accretion rates may also be attributed to the role of organic accretion, which is more important for vertical accretion than inorganic sedimentation under certain conditions (Turner et al. 2002, Morris et al. 2016). This could explain measured rates that exceed predicted rates, especially in low SSC and TR environments (Figure 2a). Therefore, our work provides empirical support to the paradigm that mineral sediment availability drives wetland vulnerability at the regional-global scale, while emphasizing that accretion rates at any particular location will be influenced by a number of other factors that cannot be predicted with simple numerical models.

## Comparison with Numerical Models

To understand potential differences between field measurements and numerical models, we used a previously published ensemble of 5 numerical models (Kirwan et al. 2010) to predict the threshold rate

of SLR that each marsh in our dataset could survive given its site-specific SSC and TR. Following Schuerch et al., (2018), the ensemble model results can be summarized as,

$$Threshold\ SLR = a * SSC * TR^{b} + c \quad (2)$$

where the constants a, b, and c equal 0.292, 0.915, and 1.5, respectively. The ensemble model indicates threshold SLR rates increase linearly with SSC for a given tidal range (Kirwan et al., 2010), which is consistent with our empirical model. However, linear regression demonstrates that the ensemble model predicts threshold SLR rates that are higher than measured accretion rates when all marshes are included (i.e., slope m= 0.57, $R^2$=0.68, $p<0.001$ where m = 1 would indicate modeled threshold rates equivalent to measured accretion rates) (Figure 3a). The analog comparison using only marshes reported as low elevation (n=41) reveals that measured accretion rates in low elevation marshes are nearly identical to modeled threshold rates of SLR for a given SSC and TR (Figure 3b; m=0.92, $R^2$=0.89, $p<0.001$).

These results illustrate a fundamental link between marsh elevation and vulnerability that may help reconcile field-based measurements of marsh accretion with numerical models of marsh survival. For example, a previous meta-analysis found that approximately 75% of marsh locations were accreting at rates less than the 7.4 mm $yr^{-1}$ rate of SLR projected under the IPCC RCP6.0 scenario and concluded that those marshes would not survive (Crosby et al., 2016). These types of observations inspire concern that numerical models overestimate accretion rates compared to what has been measured, and therefore underestimate marsh vulnerability to SLR (Parkinson et al., 2017; Jankowski et al., 2017). Indeed, we find that across our global network of sites, 40% (31 of 77) of accretion measurements are less than 7.4 mm $yr^{-1}$. Yet measured accretion rates are not themselves an indicator of the threshold rate for marsh survival because accretion rates tend to increase with flooding depth and duration (Friedrichs and Perry, 2001; Temmerman et al. 2003; Fitzgerald et al. 2008; Kirwan et al., 2016).

While a low marsh plant community that loses elevation relative to sea level is at risk of drowning, a high marsh plant community that loses elevation is at risk of first converting into a low marsh community, assuming this ecological transition is possible in the given system. When we restrict our analysis to low marsh sites, we find that less than 15% (6 of 41) of locations have accretion rates less than 7.4 mm $yr^{-1}$, and importantly, that measured low marsh accretion rates are similar to threshold rates of SLR predicted by numerical models for a given SSC and TR (Figure 3b). These results are consistent with observations of increased marsh inundation under current SLR rates, evidenced by shifts towards more flood tolerant vegetation (Donnelly and Bertness, 2001; Raposa et al., 2017), despite relatively few locations with extensive marsh drowning (Kirwan et al., 2016). Thus, our empirical analysis is consistent with numerical models that predict relatively high threshold SLR for marsh survival, albeit with significant geomorphic and ecological changes.

## Global Analysis of Critical SSC

We applied our linear regression model (eq. 1), to assess global tidal marsh vulnerability. We used our empirical model coefficients for marsh accretion and the global DIVA (Dynamic Interactive Vulnerability Assessment) database of TR, SSC, and local relative SLR rates for coastal segments that contain marshes around the world (Spencer et al., 2016; Schuerch et al., 2018). We considered the critical SSC needed for marsh accretion, based on DIVA TR and relative SLR data (eq. 1), and our empirical model coefficients that predict marsh accretion under these physical parameters. We calculated the SSC that would be required to produce accretion rates equal to the current RSLR rate using both empirical model coefficients, $C_1$=0.1624 (calculated from high marshes) and $C_1$=0.2250 (calculated from low marshes). We assume that the lower empirical model coefficient ($C_1$=0.1624) results in a critical SSC required for the marsh to maintain its current elevation relative to sea level,

206 below which high marshes become more inundated and subject to vegetation shifts (i.e. shift towards
207 more flood tolerant species). In contrast, we assume the higher coefficient ($C_1$=0.2250) to represent the
208 critical SSC for marshes to survive SLR, below which marshes drown (i.e. convert to open water).
209 Mapping of critical SSC reveals three distinct behaviors related to the maintenance of current
210 marsh elevation and the long-term survival of marshes (Figure 4). First, there are locations where SSC
211 exceeds both the critical SSC required to maintain relative elevation and the critical SSC to survive
212 relative SLR. This behavior is, for example, illustrated by marshes in Great Britain, where high tidal
213 ranges and low relative SLR rates lead to critical SSC of less than 10 mg $L^{-1}$. Estimated SSC in this
214 region are at least four times greater than the critical concentrations, and many locations have recently
215 experienced substantial marsh expansion (Ladd et al. 2019). A second behavior is when sediment supply
216 is insufficient to maintain elevation or to survive. For example, the low tidal range of western
217 Mediterranean marshes results in critical SSC greater than 100 mg $L^{-1}$ under both empirical model
218 conditions. Previous work indicates low SSC in the region and large-scale wetland loss that is consistent
219 with our empirical model predictions (Ibáñez et al., 2010; Day et al., 2011). Finally, the vulnerability
220 mapping reveals a number of locations where SSC is likely lower than the critical SSC to maintain
221 relative elevation, but higher than the critical SSC required to survive. This behavior is consistent with
222 marshes in the Northeastern United States, where accretion deficits are leading to increasing dominance
223 of flood tolerant vegetation (Donnelly and Bertness, 2001; Raposa et al., 2017), but marshes are
224 surviving SLR because accretion rates accelerate with inundation duration (Kolker et al. 2010; Wilson et
225 al., 2014).
226 To explore the effect of sea level rise on marsh vulnerability, we calculated the percentage of
227 global marsh area that would require SSC greater than a reference value under different scenarios of
228 accelerated sea level rise. Like our previous analyses, we consider both the critical SSC needed to

maintain marshes at their current elevation, and the critical SSC needed for marshes to survive. We use 30 mg $L^{-1}$ as a reference value as the median SSC of our dataset is 33 mg $L^{-1}$ and the average SSC for U.S. coastal rivers is 30.3 mg $L^{-1}$ (Weston 2014). Concentrations of suspended sediment are declining in rivers throughout the world (Wang et al., 2011; Weston 2014), meaning this reference value may not be representative of average SSC in the future. We find that approximately 35% of global marsh area requires SSC > 30 mg $L^{-1}$ to maintain elevation under the current rate of eustatic SLR (3 mm $yr^{-1}$), and that the percentage increases to 60% at SLR rates of 10 mm $yr^{-1}$ (Figure 4a). However, to survive current SLR (3 mm $yr^{-1}$) only 24% of global marsh area requires SSC > 30 mg $L^{-1}$, increasing to 48% at high rates of SLR (10 mm $yr^{-1}$) (Figure 4b). This global analysis suggests that the threshold SLR rates allowing maintenance of marsh elevation are much lower than those allowing marsh survival, assuming that high marshes are capable of the ecological transition to low marshes. While many other factors (e.g. organic accretion, shallow subsidence) influence local marsh survival, measured accretion rates in low marshes are consistent with modeled threshold rates of SLR for a given TR and SSC (Figure 3b). Together, these results help bridge the gap between numerical models and field measurements, and suggest that threshold rates of SLR can be predicted primarily by physical factors at the regional to global scale.

## Supplementary Material

### Direct measurements of SSC and vertical accretion

We measured SSC and vertical accretion at seven tidal marsh sites spanning the eastern coast of the US and one on the eastern coast of Australia. Four of these sites were located within extremely low elevation, youthful marshes, at Plum Island Ecosystems Long Term Ecological Research station (PIE LTER), Virginia Coastal Reserve LTER (VCR LTER), Chesapeake Bay National Estuarine Research

Reserve (CB NERR), and Georgia Coastal Ecosystems LTER (GCE LTER), respectively (Figure 1). We conducted long term turbidity measurements on the marsh platform, site-specific SSC calibrations, and direct accretion measurements at these four low marsh sites. The three additional sites were monitored for shorter durations (maximum=2 months) and either relied on measurements from other studies or were at higher elevations. All monitored sites were included within the meta-analysis.

Optical backscatter turbidity probes were deployed on the marsh platform and in the adjacent tidal creek to determine the channel SSC and average SSC for the marsh. Our basic approach to measuring SSC follows methods described in previous work at the GCE LTER and PIE LTER (Coleman and Kirwan, 2019; Coleman et al., 2020), where 3-6 sensors were deployed across a transect from tidal channel to marsh interior, measuring turbidity every 15 minutes for the length of the deployment (1-15 months). Pressure transducers were used to calculate water depth, which was used to estimate tidal range and to remove data points corresponding to time periods when the marsh was not flooded. Turbidity was converted to SSC via *in situ* field calibrations and lab calibrations with native sediment from each site (Coleman and Kirwan, 2019). All calibration equations are in the form of SSC=Turbidity*Calibration Coefficient. The calibration coefficients for the PIE LTER, VCR LTER, CB NERR, and GCE LTER are 2.26 ($R^2$=0.98), 1.31 ($R^2$=0.99), 1.04 ($R^2$=0.98), and 1.33 ($R^2$=0.93), respectively. Suspect data points were removed from the SSC time series following Ganju et al. (2005). These points represent times when the sensor may have been obstructed by vegetation, or subject to fouling. The SSC time series demonstrate distinct tidal patterns and changes in concentration with distance into the marsh (see Coleman and Kirwan, 2019; Coleman et al., 2020; Supplementary Figure 2). Nevertheless, here we define the SSC of each site simply as the average over-marsh concentration calculated from the entire record of all marsh sensors at a given site.

We measured short-term accretion using sediment tiles made of 14.5 cm x 14.5 cm plastic grids with 1.5 $cm^2$ openings cut from fluorescent tube lighting covers installed flush to the marsh surface (Coleman et al., 2019). These grids allow plants to grow through them and represent a natural surface for sediment accumulation. On subsequent visits to the sites, we measured the thickness of sediment that had accumulated on the grid to calculate an accretion rate. Sediment tile deployments varied in length, from 9-24 months.

Long-term accretion rates were calculated from the vertical distribution of excess Pb-210 ($^{210}Pb_{xs}$) in sediment cores (15 cm diameter x 100 cm length) collected from each study sites. Each core was sectioned at 1-cm interval with a subset of intervals (every other sample for top 20 cm and every fourth sample beyond 20 cm) prepared for radiometric analysis. Briefly, each interval was dried, pulverized, quantitatively spiked with 6.0 dpm (100 mBq) of polonium-209 ($^{209}Po$), and reacted with hot (nitric and hydrochloric) acids to leach $^{210}Po$ (granddaughter of $^{210}Pb$) from sediments. Leachate was conditioned following a modified procedure of Flynn (1968) (also reviewed by Sethy et al. 2015) to promote the spontaneous deposition of Po-isotopes on silver (Ag) planchets. The planchets were measured on alpha spectrometry to quantify both $^{209}Po$ (4.86 MeV) and $^{210}Po$ (5.41 MeV) isotopes. Leachable $^{210}Po$ (and $^{210}Pb$) was quantified by multiplying the $^{209}Po$ activity-to-count rate-ratio by the $^{210}Po$ count rate. Excess $^{210}Pb$ was assumed to be in secular equilibrium and thus equivalent to acid-leached polonium-210 ($^{210}Po$). Average accretion rates were estimated using log-linear relationships between $^{210}Pb_{xs}$ and depth in the core following Robbins et al. (1975). Mid-depth samples (four to five samples between approximately 15 and 45 cm in select cores) were also analyzed for cesium-137 ($^{137}Cs$) to corroborate and/or supplement $^{210}Pb_{xs}$-based accretion rates. Dry and pulverized samples were sealed in a container and measured on a Canberra (now Mirion Technologies, Inc.) Low-Energy, Germanium (LeGe) detector using the 661.7 keV photopeak. Self-absorption correction for samples followed Cutshall et al. (1983).

297 The four low marsh monitored sites (Supplementary Table 2) ranged in over-marsh SSC from
298 approximately 5-30 mg $L^{-1}$, TR from 1.1-3.6 m, and accretion rate from approximately 7-27 mm $yr^{-1}$.
299 Spatially, SSC was highest in the tidal channel at all sites, except for the CB NERR site which has a
300 sandy berm proximal to the marsh interior sensor. Temporally, SSC tended to be the highest at mid-tide,
301 presumably coincident with the fastest flow velocities. The sites at the PIE LTER and the CB NERR had
302 the lowest SSC (5.2 and 13.4 mg $L^{-1}$, respectively) and lower accretion rates, which were successfully
303 determined with Pb-210 (6.6 and 7.3 mm $yr^{-1}$, respectively; Supplementary Figure 3). SSC was higher at
304 the VCR LTER (27.7 mg $L^{-1}$) and GCE LTER (31 mg $L^{-1}$), but accretion rates could not be determined
305 with radiochronology methods because the sites were accreting too rapidly or experienced erosion.
306 Instead, we calculated accretion rates at these sites from sediment grids (27 and 24 mm $yr^{-1}$,
307 respectively; Supplementary Figure 4). These short-term accretion rates were verified by comparing
308 them to other studies in the system and estimates of accretion based on the timing of vegetation
309 colonization in aerial photographs and changes in organic content, bulk density, and water content
310 observed in sediment cores. The accretion rate of all four sites were greater than the local relative SLR
311 rate and similar to numerical model-predicted threshold SLR rates.
312
313 **Meta-analysis and Empirical Model Formulation**
314 Data from the literature was compiled to include a wider range of salinities, vegetation types,
315 elevations, SSC, TR, and accretion. We included data from an additional 70 tidal marshes (for a total of
316 77 sites) where there were direct measurements of SSC and accretion from around the world
317 (Supplementary Table 1). The greatest concentration of sites was in Europe and North America. The
318 sites had a range of SSC of 0.5-358 mg $L^{-1}$, TR of 0.3-12 m, and accretion rates of 1-400 mm $yr^{-1}$. In

situations where SSC and accretion data came from different sources, sites were only included if measurements were conducted within 2 km and 15 years from one another.

We removed outliers from the significant linear relationship between SSC*TR and accretion (eq. 1) to determine the empirical model coefficient most useful for fitting the data to a linear trend. First, all points were used for creating a linear model between SSC*TR and accretion; then, we identified the data point with the largest residual error and calculated a new linear model excluding this data point. Data points were removed in sequence until the removal of an additional outlier had a negligible effect on the slope of the relationship between SSC*TR and accretion based on an analysis of the derivative of the change in slope with the number of outliers removed. Removing 5 of the 77 marsh sites was deemed most appropriate. This approach removes variability from the linear regression so that the resulting slope ($C_1$) is representative of the majority of the data but not overly influenced by extreme data points.

We analyzed several potential equations to determine the best empirical relationship between SSC, TR, and vertical accretion (Supplementary Table 3). The simplest empirical equation is analogous to a fixed proportion of the sediment suspended in the flooding waters being converted to vertical marsh accretion (equation 1). We then binned marsh sites into 6 groups based on spring tidal range. A plot of the slope of linear regressions between measured accretion and SSC*TR for each tidal range group appeared as a logistic curve, which was then used to define a second model (Supplementary Table 3). For a third empirical model, we determined the best fit linear model (Supplementary Table 3). The simplistic equation predicted accretion as well as the two more complex equations (Supplementary Table 3).

## Influence of Different Methodology

Accretion rates and SSC measurements vary with timescale and location of sampling (Christiansen et al., 2000; Parkinson et al. 2016; Breithaupt et al., 2018; Coleman et al., 2020) so we analyzed the relationship between SSC and vertical accretion separately for different methods of measuring accretion and SSC. Accretion methods were classified as radiochronology (Pb210, Cs137), modern sediment deposition (sediment tiles and marker horizons), or modern elevation change (surface elevation tables). We distinguished between measurements of SSC made with bottle sampling and automated sensors, and between measurements made in the channel and over the flooded marsh. For each methodological approach, we calculated the slope between measured accretion and SSC*TR ($C_1$ in equation 1).

The slope calculated using modern accretion rates was slightly greater but not significantly different than the slope calculated using elevation change rates (modern accretion $C_1$=0.2452 ± 0.009; elevation change $C_1$=0.1980 ± 0.019; Figure 2b). The main difference between these approaches is that shallow subsidence is incorporated into elevation change measurements but not accretion measurements (Cahoon et al., 1995; Cahoon et al. 2006; Jankowski et al. 2017). Our results therefore suggest that shallow subsidence is not a significant contributor to short-term elevation change for a given TR and SSC at the spatial scales and levels of observational uncertainty considered in our study. The slope calculated using only radiochronological measurements was significantly lower than that derived from other approaches ($C_1$=0.1014 ± 0.008), indicating that accretion rates measured over long timescales are lower than rates measured over short timescales for a given SSC and TR. Our work therefore adds to the growing body of literature identifying a "timescale bias" in which apparent accretion rates decrease with increasing timescale (Breithaupt et al., 2018). Lower apparent accretion rates could be explained by accretion rates that decline as youthful marshes approach an equilibrium elevation (Redfield, 1972), a longer period of time for compaction and organic matter decomposition (Bartholdy et al., 2010), and/or

364 accretion rates averaged over periods of time with slower SLR (Kirwan et al., 2016). The impacts of
365 shallow subsidence are likely being masked by the variability in accretion rates between sites, whereas
366 the impact of long-term subsidence may be too large to be masked by inter-marsh variability. In any
367 case, our finding that accretion rates are significantly lower when measured over longer timescales is
368 consistent with previous work that highlights the influence of long-term subsurface elevation loss in
369 long-term accretion rates (Kearney et al., 2004; Bartholdy et al., 2010; Tornqvist et al., 2008; Horton et
370 al. 2018; Tornqvist et al. 2020; Saintilan et al. 2020), as well as the observation that accretion rates have
371 increased in response to the recent acceleration in the rate of SLR (Kolker et al., 2010; Hill and Anisfeld
372 2015). Short-term accretion rates potentially underestimate marsh vulnerability because they do not fully
373 account for subsurface processes that manifest over longer time periods (Parkinson et al., 2017),
374 whereas long-term accretion rates overestimate marsh vulnerability because accretion rates increase in
375 response to accelerating rates of SLR (Kirwan et al., 2017). Since the best approach for assessing
376 wetland vulnerability is unclear (Breithaupt et al., 2018), we incorporate both long-term and short-term
377 measurements of accretion in our empirical modeling (Figures 2 and 3). This approach allows us to
378 quantify the impact of different methods over a broad range of environmental conditions and shows that
379 methodological differences increase with greater sediment availability and more rapid rates of accretion
380 (Figure 2b).

381 We also explored how the relationship between accretion and SSC*TR depends on differences in
382 the SSC measurement methodology. Sites were grouped based on whether SSC was measured via bottle
383 sampling or automated sensors, and whether SSC measurements were made in the channel or over the
384 flooded marsh. Although the different SSC measurement approaches had different values of $C_1$, it is
385 difficult to determine how generalizable the results are (Supplementary Figure 5). Measurements made
386 by sensors and measurements over the marsh (n=31; n=16) were less common and covered a narrower

range of SSC values than measurements made with bottle sampling and in the channel (n=46; n=61). Although previous work suggests strong temporal variability in SSC that may only be captured with sensors or sampling over long durations (Coleman et al., 2020), and strong spatial gradients between SSC measured in channels and SSC across the marsh platform (Christiansen et al., 2000; Leonard and Reed, 2002; Poirier et al., 2017), there was insufficient information to sufficiently understand the effect of SSC methodology on the relationship between accretion and SSC. We consequently combined all SSC measurement methods in our meta-analysis and empirical modeling, and note that significant trends between accretion and SSC emerge despite this potential variability.

## Global Analysis Methodology

The global modelling of sediment balances is based on the Global Coastal Wetland Model by Schuerch et al. (2018). This relies on the global database from the DIVA including TR and areal coastal wetland data (McOwen et al., 2017), attributed to a total of 12,148 coastline segment of varying length (depending on bio-physical and socio-economic coastline characteristics; Spencer et al., 2016). Spring tidal range data was derived from a new global tidal range dataset (Pickering et al. 2017) using the global tide model OTISmpi (Egbert et al., 2004). Mean spring high water levels and mean spring low water levels were retrieved from a 15-day sea-level reconstruction based on the tidal constituents M2, S2, K1 and O1 (Schuerch et al. 2018).

Our initial goal was to use the empirical model to calculate the spatial extent of expected marsh drowning under different SLR rates. However, we found that the GlobColour satellite-derived SSC data used by DIVA database was considerably lower than and inconsistently related to the SSC in our meta-analysis (Supplementary Figure 1). We suggest that this discrepancy is due to the resolution of the satellite data (4.6km; GlobColour, 2020), which presumably includes low-SSC waters further offshore.

410 This suggests limitations in predicting global threshold rates of SLR and that previous estimates of
411 marsh vulnerability (e.g. Schurech et al., 2018) may be conservative. We instead consider the critical
412 SSC needed for marsh accretion, based on DIVA TR and relative SLR data, and our empirical model
413 coefficients that predict marsh accretion under these physical parameters.

414 Critical SSC for each coastline segment was calculated as a function of spring TR and global
415 sea-level rise for current (3 mm $yr^{-1}$) and accelerated rates (6 and 10 mm $yr^{-1}$). Global sea-level rise rates
416 were adjusted by regional vertical land movement due to glacial isostatic adjustment (Peltier et al.,
417 2004) and accelerated land subsidence in delta regions (2 mm $yr^{-1}$ for every delta in the database) to
418 derive regional relative sea-level rise (RSLR) rates. Based on equation 1, and assuming that the
419 maximum possible accretion rate equals RSLR, critical SSC was calculated as follows:

420 $$SSC_{crit} = RSLR/(C_1 * TR) \quad (3)$$

421 The resulting $SSC_{crit}$ values were binned into five categories for which total saltmarsh areas were
422 calculated.

423 To explore the effect of SLR on marsh vulnerability, we calculated the percentage of global
424 marsh area that would require SSC greater than a reference value under different scenarios of
425 accelerated SLR. Like our previous analyses, we consider both the critical SSC needed to maintain
426 marshes at their current elevation, and the critical SSC needed for marshes to survive. We use 30 mg $L^{-1}$
427 as a reference value as the median SSC of our dataset is 33 mg $L^{-1}$ and the average SSC for U.S. coastal
428 rivers is 30.3 mg $L^{-1}$ (Weston 2014). Concentrations of suspended sediment is declining in rivers
429 throughout the world (Wang et al., 2011; Weston 2014), meaning this reference value may not be
430 representative of average SSC in the future. We find that approximately 35% of global marsh area
431 requires SSC > 30 mg $L^{-1}$ to maintain elevation under the current rate of eustatic SLR (3 mm $yr^{-1}$), and
432 that this percentage increases with SLR (i.e. 60% at 10 mm $yr^{-1}$) (Figure 4a). However, to survive

current SLR (3 mm $yr^{-1}$) only 24% of global marsh area requires SSC > 30 mg $L^{-1}$, increasing to 48% at high rates of SLR (10 mm $yr^{-1}$) (Figure 4b).


## Acknowledgements

This work was funded by the U.S. Geological Survey Land Change Science Climate R&D Program. Additional funding was provided through The National Science Foundation (NSF) Graduate Research Fellowship Program, NSF LTER #1832221, NSF EAR-CAREER #1654374, NSF EAR-GLD #1529245, and NSF OCE-SEES #1426981. GRG acknowledges support from the U.S. Geological Survey Ecosystems Mission Area. The authors would like to thank the many researchers who provided valuable data, including W. Wagner, D. von Proosdij, C. Lovelock, K. Rogers, C. Ladd, and J. Raw. We would also like to thank J. Green, D. Walters, J. Himmelstein, D. Nicks, R. Walker, T. Messershmidt, N. Schieder, and the staff of the PIE LTER, GCE LTER, VCR LTER, and CB NERR for their assistance in data collection. Any use of trade, firm, or product names is for descriptive purposes only and does not imply endorsement by the US Government. This is contribution no. XXXX of the Virginia Institute of Marine Science

## References


Bartholdy, J., Pedersen, J. B. T., & Bartholdy, A. T. (2010). Autocompaction of shallow silty salt marsh clay. *Sedimentary Geology*, *223*(3-4), 310-319.

Breithaupt, J. L., Smoak, J. M., Byrne, R. H., Waters, M. N., Moyer, R. P., & Sanders, C. J. (2018). Avoiding timescale bias in assessments of coastal wetland vertical change. *Limnology and oceanography*, *63*(S1), S477-S495.

Bricker-Urso, S., Nixon, S. W., Cochran, J. K., Hirschberg, D. J., & Hunt, C. (1989). Accretion rates and sediment accumulation in Rhode Island salt marshes. *Estuaries*, *12*(4), 300-317.

Cadol, D., Engelhardt, K., Elmore, A., & Sanders, G. (2014). Elevation-dependent surface elevation gain in a tidal freshwater marsh and implications for marsh persistence. *Limnology and Oceanography*, *59*(3), 1065-1080.

Cahoon, D. R., Hensel, P. F., Spencer, T., Reed, D. J., McKee, K. L., & Saintilan, N. (2006). Coastal wetland vulnerability to relative sea-level rise: wetland elevation trends and process controls. In *Wetlands and natural resource management* (pp. 271-292). Springer, Berlin, Heidelberg.

Cahoon, D. R., Reed, D. J., & Day Jr, J. W. (1995). Estimating shallow subsidence in microtidal salt marshes of the southeastern United States: Kaye and Barghoorn revisited. *Marine geology*, *128*(1-2), 1-9.

Christiansen, T., Wiberg, P. L., & Milligan, T. G., (2000). Flow and sediment transport on a tidal salt marsh surface. *Estuarine, Coastal and Shelf Science 50*(3), 315-331

Chmura, G. L., and G. A. Hung (2004), Controls on salt marsh accretion: A test in salt marshes of eastern Canada, Estuaries, 27, 70–81

Church, J.A., P.U. Clark, A. Cazenave, J.M. Gregory, S. Jevrejeva, A. Levermann, M.A. Merrifield, G.A. Milne, R.S. Nerem, P.D. Nunn, A.J. Payne, W.T. Pfeffer, D. Stammer and A.S.

Unnikrishnan, (2013). Sea Level Change. In: Climate Change 2013: The Physical Science Basis. Contribution of Working Group I to the Fifth Assessment Report of the Intergovernmental Panel on Climate Change [Stocker, T.F., D. Qin, G.-K. Plattner, M. Tignor, S.K. Allen, J. Boschung, A. Nauels, Y. Xia, V. Bex and P.M. Midgley (eds.)]. Cambridge University Press, Cambridge, United Kingdom and New York, NY, USA.

Coleman, D.J., & Kirwan, M.L., (2019). The effect of a small vegetation dieback event on salt marsh sediment transport. *Earth Surface Processes and Landforms* 44(4), 944-952, https://doi.org/10.1002/esp.4547

Coleman, D. J., Ganju, N. K., and Kirwan, M. L., (2020) Sediment delivery to a tidal marsh platform is minimized by source decoupling and flux convergence. *Journal of Geophysical Research—Earth Surface, 125(8), e2020JF005558*.

Crosby, S. C., Sax, D. F., Palmer, M. E., Booth, H. S., Deegan, L. A., Bertness, M. D., & Leslie, H. M. (2016). Salt marsh persistence is threatened by predicted sea-level rise. *Estuarine, Coastal and Shelf Science*, *181*, 93-99.

Cutshall, N. H., I. L. Larsen, and C. R. Olsen (1983), Direct analysis of 210Pb in sediment samples: Self-absorption corrections, *Nuclear Instruments & Methods B*, *206*, 309-312.

D'Alpaos, A., & Marani, M., (2016). Reading the signatures of biologic–geomorphic feedbacks in salt-marsh landscapes. *Advances in Water Resources 93b* 265-275

Day, J., Ibáñez, C., Scarton, F., Pont, D., Hensel, P., Day, J., & Lane, R. (2011). Sustainability of Mediterranean deltaic and lagoon wetlands with sea-level rise: the importance of river input. *Estuaries and Coasts*, *34*(3), 483-493.

DeLaune, R. D., Patrick, W. H., & Buresh, R. J. (1978). Sedimentation rates determined by 137 Cs dating in a rapidly accreting salt marsh. *Nature*, *275*(5680), 532-533.

503 Dieng, H. B., Cazenave, A., Meyssignac, B., & Ablain, M. (2017). New estimate of the current rate of
504 sea level rise from a sea level budget approach. *Geophysical Research Letters*, *44*(8), 3744-3751.
505 Donnelly, J. P., & Bertness, M. D. (2001). Rapid shoreward encroachment of salt marsh cordgrass in
506 response to accelerated sea-level rise. *Proceedings of the National Academy of Sciences*, *98*(25),
507 14218-14223.
508 Duvall, M. S., Wiberg, P. L., & Kirwan M. L., (2019). Controls on sediment suspension, flux, and marsh
509 deposition near a bay-marsh boundary. *Estuaries and Coasts 42*(2) 403-424,
510 https://doi.org/10.1007/s12237-018-0478-4
511 Egbert, G. D., Ray, R. D. & Bills, B. G. Numerical modeling of the global semidiurnal tide in the
512 present day and in the last glacial maximum. J. Geophys. Res. Oceans 109, C03003 (2004).
513 Ensign, S., Currin, C., Piehler, M., & Tobias, C. (2017). A method for using shoreline morphology to
514 predict suspended sediment concentration in tidal creeks. *Geomorphology*, *276*, 280-288.
515 Fagherazzi, S., Kirwan, M. L., Mudd, S. M., Guntenspergen, G. R., Temmerman, S., D'Alpaos, A., ... &
516 Clough, J. (2012). Numerical models of salt marsh evolution: Ecological, geomorphic, and
517 climatic factors. Reviews of Geophysics, 50(1).FitzGerald, D. M., Fenster, M. S., Argow, B. A.,
518 & Buynevich, I. V. (2008). Coastal impacts due to sea-level rise. *Annual Review of Earth and*
519 *Planetary Sciences*, *36*.
520 Flynn, W. W. (1968), The determination of low levels of polonium-210 in environmental materials,
521 *Analytica Chimica Acta*, *43*, 221-227.
522 French, J. (2006), Tidal marsh sedimentation and resilience to environmental change: Exploratory
523 modeling of tidal, sea-level, and sediment supply forcing in predominantly allochthonous
524 systems, Mar. Geol., 235, 119–136

525 Friedrichs, C. T., & Perry, J. E. (2001). Tidal salt marsh morphodynamics: a synthesis. *Journal of*
526 *Coastal Research*, 7-37.
527 Ganju, N. K., Defne, Z., Kirwan, M. L., Fagherazzi, S., D'Alpaos, A., & Carniello, L. (2017). Spatially
528 integrative metrics reveal hidden vulnerability of microtidal salt marshes. *Nature*
529 *Communications*, *8*(1), 1-7.
530 Ganju N. K., Kirwan M. L., Dickhudt P. J., Guntenspergen G. R., Cahoon D. R., & Kroeger K. D.,
531 (2015). Sediment transport-based metrics of wetland stability. *Geophysical Research Letters*
532 *42*(19), 7992-8000.
533 Ganju, N.K., Schoellhamer, D.H. & Bergamaschi, B.A., (2005). Suspended sediment fluxes in a tidal
534 wetland: Measurement, controlling factors, and error analysis. *Estuaries 28*(6), 812-822.
535 GlobColour (2020). Product User's Guide. Version 4.2, Reference GC-UM-ACR-PUG-01
536 Harrison, E. Z., and A. L. Bloom (1977), Sedimentation rates on tidal salt marshes in Connecticut, J.
537 Sediment. Petrol., 47, 1484–1490
538 Hill, T. D., & Anisfeld, S. C. (2015). Coastal wetland response to sea level rise in Connecticut and New
539 York. *Estuarine, Coastal and Shelf Science*, *163*, 185-193.
540 Horton, B.P., Shennan, I., Bradley, S.L. et al. (2018). Predicting marsh vulnerability to sea-level rise
541 using Holocene relative sea-level data. *Nature Communications 9*(2687)
542 https://doi.org/10.1038/s41467-018-05080-0
543 Ibáñez, C., Sharpe, P. J., Day, J. W., Day, J. N., & Prat, N. (2010). Vertical accretion and relative sea
544 level rise in the Ebro Delta wetlands (Catalonia, Spain). *Wetlands*, *30*(5), 979-988.
545 Jankowski, K. L., Törnqvist, T. E., & Fernandes, A. M. (2017). Vulnerability of Louisiana's coastal
546 wetlands to present-day rates of relative sea-level rise. *Nature Communications*, *8*(1), 1-7.

547 Kearney, M. S., Stevenson, J. C., & Ward, L. G. (1994). Spatial and temporal changes in marsh vertical
548 accretion rates at Monie Bay: Implications for sea-level rise. *Journal of Coastal Research*, 1010-
549 1020.
550 Kirwan, M. L., & Guntenspergen, G. R. (2010). Influence of tidal range on the stability of coastal
551 marshland. *Journal of Geophysical Research: Earth Surface*, *115*(F2).
552 Kirwan, M. L., & Megonigal, J. P. (2013). Tidal wetland stability in the face of human impacts and sea-
553 level rise. *Nature*, *504*(7478), 53-60.
554 Kirwan, M., & Temmerman, S. (2009). Coastal marsh response to historical and future sea-level
555 acceleration. *Quaternary Science Reviews*, *28*(17-18), 1801-1808.
556 Kirwan, M. L., Temmerman, S., Guntenspergen, G. R., & Fagherazzi, S. (2017). Reply to 'Marsh
557 vulnerability to sea-level rise'. *Nature Climate Change*, *7*(11), 756-757.
558 Kirwan, M. L., Temmerman, S., Skeehan, E. E., Guntenspergen, G. R., & Fagherazzi, S. (2016).
559 Overestimation of marsh vulnerability to sea level rise. *Nature Climate Change*, *6*(3), 253-260.
560 Kolker, A. S., Kirwan, M. L., Goodbred, S. L., & Cochran, J. K. (2010). Global climate changes
561 recorded in coastal wetland sediments: empirical observations linked to theoretical
562 predictions. *Geophysical Research Letters*, *37*(14).
563 Ladd, C. J., Duggan-Edwards, M. F., Bouma, T. J., Pagès, J. F., & Skov, M. W. (2019). Sediment supply
564 explains long-term and large-scale patterns in salt marsh lateral expansion and
565 erosion. *Geophysical Research Letters*, *46*(20), 11178-11187.
566 Leonard, L. A., & Reed D. J. (2002). Hydrodynamics and sediment transport through tidal marsh
567 canopies. *Journal of Coastal Research S.I.36*, 459 – 469.

568 Marani, M., D'Alpaos, A., Lanzoni, S., Carniello, L., & Rinaldo, A. (2007). Biologically-controlled
569 multiple equilibria of tidal landforms and the fate of the Venice lagoon. *Geophysical Research*
570 *Letters*, *34*(11).
571 Mariotti, G. (2020). Beyond marsh drowning: The many faces of marsh loss (and gain). *Advances in*
572 *Water Resources*, *144*, 103710.
573 McOwen, C. et al. A global map of saltmarshes. Biodivers. Data J. 5, e11764 (2017).
574 Morris, J. T., Barber, D. C., Callaway, J. C., Chambers, R., Hagen, S. C., Hopkinson, C. S., ... &
575 Wigand, C. (2016). Contributions of organic and inorganic matter to sediment volume and
576 accretion in tidal wetlands at steady state. *Earth's future*, *4*(4), 110-121.
577 Moskalski, S. M. & Sommerfield, C. K. (2012). Suspended sediment deposition and trapping efficiency
578 in a Delaware salt Marsh. Geomorphology 139-140, 195-204.
579 Mudd, S. M., Fagherazzi, S., Morris, J. T., & Furbish, D. J. (2004). Flow, sedimentation, and biomass
580 production on a vegetated salt marsh in South Carolina: toward a predictive model of marsh
581 morphologic and ecologic evolution. *The Ecogeomorphology of Tidal Marshes, Coastal*
582 *Estuarine Stud*, *59*, 165-187.
583 Murphy, S., & Voulgaris G., (2006). Identifying the role of tides, rainfall and seasonality in marsh
584 sedimentation using long-term suspended sediment concentration data. *Marine Geology 227*(1-2)
585 31-50,
586 Palinkas, C. M. & Engelhardt, K. A. M., (2018). Influence of inundation and suspended-sediment
587 concentrations on spatiotemporal sedimentation patterns in a tidal freshwater marsh. *Wetlands*
588 Parkinson, R. W., Craft, C., DeLaune, R. D., Donoghue, J. F., Kearney, M., Meeder, J. F., ... & Turner,
589 R. E. (2017). Marsh vulnerability to sea-level rise. *Nature Climate Change*, *7*(11), 756-756.

590 Peltier, W. Global glacial isostasy and the surface of the ice-age earth: the ice-5G (VM2) model and
591 GRACE. Annu. Rev. Earth Planet. Sci. 32, 111–149 (2004).
592 Pickering, M. D. et al. The impact of future sea-level rise on the global tides. Cont. Shelf Res. 142, 50–
593 68 (2017).
594 Poirier, E., van Proosdij, D., & Milligan, T.G., (2017). The effect of source suspended sediment
595 concentration on the sediment dynamics of a macrotidal creek and salt marsh. *Continental Shelf*
596 *Research 148* 130-138.
597 Raposa, K. B., Weber, R. L., Ekberg, M. C., & Ferguson, W. (2017). Vegetation dynamics in Rhode
598 Island salt marshes during a period of accelerating sea level rise and extreme sea level
599 events. *Estuaries and Coasts*, *40*(3), 640-650.
600 Redfield, A. C. (1972). Development of a New England salt marsh. Ecological monographs, 42(2), 201-
601 237.
602 Reed, D. J. (1995). The response of coastal marshes to sea-level rise: Survival or submergence?. *Earth*
603 *Surface Processes and Landforms*, *20*(1), 39-48.
604 Robbins, J. A., and D. N. Edgington (1975), Determination of recent sedimentation rates in Lake
605 Michigan using Pb-210 and Cs-137, *Geochimica et Cosmochimica Acta*, *39*(3), 285-304.
606 Saintilan, N., Khan, N. S., Ashe, E., Kelleway, J. J., Rogers, K., Woodroffe, C. D., Horton, B. P., (2020)
607 Thresholds of mangrove survival under rapid sea level rise. *Science 368*(6495) 1118-1121
608 Schuerch, M., Rapaglia, J., Liebetrau, V., Vafeidis, A., & Reise, K. (2012). Salt marsh accretion and
609 storm tide variation: an example from a barrier island in the North Sea. *Estuaries and*
610 *Coasts*, *35*(2), 486-500.
611 Schuerch, M., Spencer, T., Temmerman, S., Kirwan, M. L., Wolff, C., Lincke, D., ... & Hinkel, J.
612 (2018). Future response of global coastal wetlands to sea-level rise. *Nature*, *561*(7722), 231-234.

613 Schuerch, M., Vafeidis, A., Slawig, T., & Temmerman, S. (2013). Modeling the influence of changing
614 storm patterns on the ability of a salt marsh to keep pace with sea level rise. *Journal of*
615 *Geophysical Research: Earth Surface*, *118*(1), 84-96.
616 Sethy, N. K., A. K. Sutar, P. Rath, V. N. Jha, P. M. Ravi, and R. M. Tripathi (2015), A review of radio
617 chemical analysis and estimation of 210Po in soil matrices, *Journal of Radiation Research and*
618 *Applied Sciences*, *8*(4), 590-596.
619 Spencer, T., Schuerch, M., Nicholls, R. J., Hinkel, J., Lincke, D., Vafeidis, A. T., ... & Brown, S. (2016).
620 Global coastal wetland change under sea-level rise and related stresses: The DIVA Wetland
621 Change Model. *Global and Planetary Change*, *139*, 15-30.
622 Stevenson, J. C., Ward, L. G., & Kearney, M. S. (1986). Vertical accretion in marshes with varying rates
623 of sea level rise. In *Estuarine variability* (pp. 241-259). Academic Press.
624 Stoddart, D. R., Reed, D. J., & French, J. R. (1989). Understanding salt-marsh accretion, Scolt Head
625 Island, Norfolk, England. *Estuaries*, *12*(4), 228-236.
626 Temmerman, S., Govers, G., Meire, P., & Wartel, S. (2003). Modelling long-term tidal marsh growth
627 under changing tidal conditions and suspended sediment concentrations, Scheldt estuary,
628 Belgium. *Marine Geology*, *193*(1-2), 151-169.
629 Törnqvist, T. E., Wallace, D. J., Storms, J. E., Wallinga, J., Van Dam, R. L., Blaauw, M., ... & Snijders,
630 E. M. (2008). Mississippi Delta subsidence primarily caused by compaction of Holocene
631 strata. *Nature Geoscience*, *1*(3), 173-176.
632 Törnqvist, T. E., Cahoon, D. R., Day, J. W., & Morris, J. T. (2019). Global coastal wetland expansion
633 under accelerated sea-level rise is unlikely. *EarthArXiv* https://doi.org/10.31223/osf.io/d2nhs
634 Törnqvist, T. E., Jankowski, K. L., Li, Y., Gonzalez, J. L., (2020). Tipping points of Mississippi Delta
635 marshes due to accelerated sea-level rise. *Science Advances 6*(21) 10.1126/sciadv.aaz5512

636 Turner, R. E., Swenson, E. M., & Milan, C. S. (2002). Organic and inorganic contributions to vertical
637 accretion in salt marsh sediments. In *Concepts and controversies in tidal marsh ecology* (pp.
638 583-595). Springer, Dordrecht.
639 Wang, H., Saito, Y., Zhang, Y., Bi, N., Sun, X., & Yang, Z. (2011). Recent changes of sediment flux to
640 the western Pacific Ocean from major rivers in East and Southeast Asia. *Earth-Science*
641 *Reviews*, *108*(1-2), 80-100.
642 Watson, E. B., Raposa, K. B., Carey, J. C., Wigand, C., & Warren, R. S. (2017). Anthropocene survival
643 of southern New England's salt marshes. *Estuaries and Coasts*, *40*(3), 617-625.
644 Weston, N. B. (2014). Declining sediments and rising seas: an unfortunate convergence for tidal
645 wetlands. *Estuaries and Coasts*, *37*(1), 1-23.
646 Wiberg, P. L., Fagherazzi, S., & Kirwan, M. L. (2020). Improving predictions of salt marsh evolution
647 through better integration of data and models. *Annual review of marine science*, *12*, 389-413.
648 Wilson, C. A., Hughes, Z. J., FitzGerald, D. M., Hopkinson, C. S., Valentine, V., & Kolker, A. S.
649 (2014). Saltmarsh pool and tidal creek morphodynamics: Dynamic equilibrium of northern
650 latitude saltmarshes?. *Geomorphology*, *213*, 99-115.

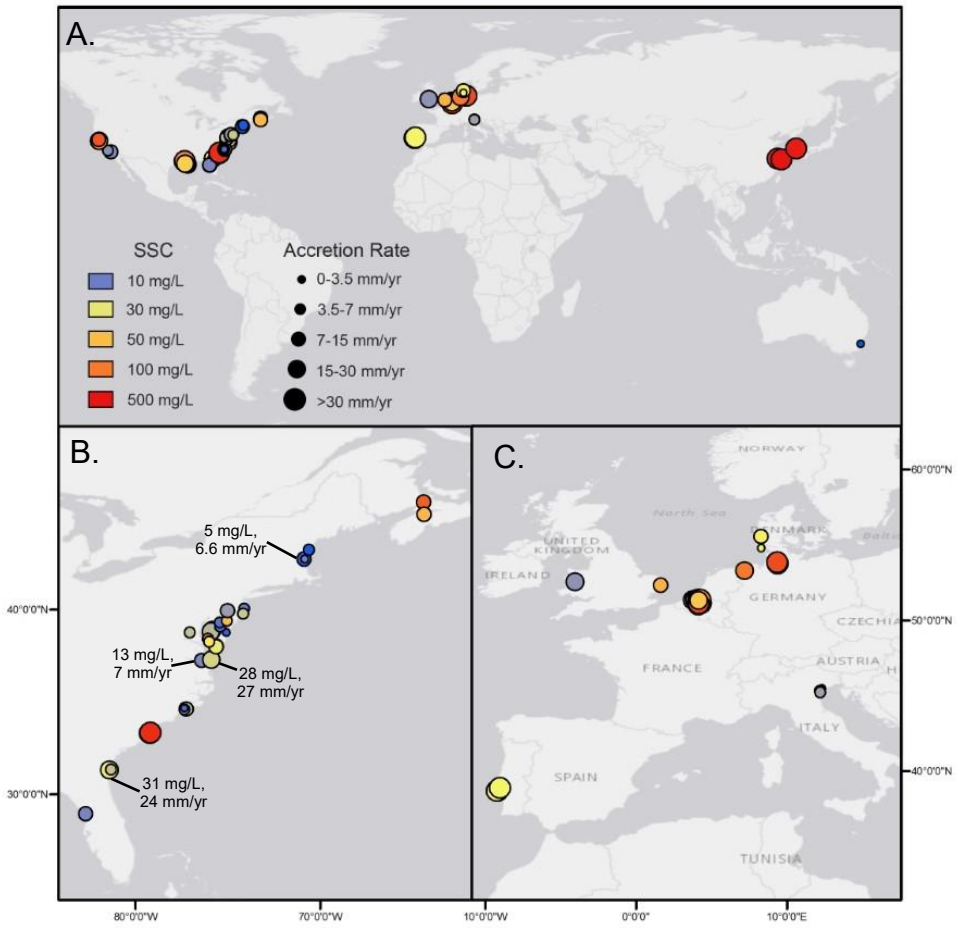


Figure 1: A. Site map showing SSC and accretion rates of sites used in the meta-analysis. Warmer colors indicate higher SSC and reference values are displayed in the legend. Size of the circle represents accretion rate, with larger circles indicating greater accretion rates. B. Magnified view of the east coast of North America and C. Western Europe, with labels indicating SSC and accretion of low marsh monitoring sites.

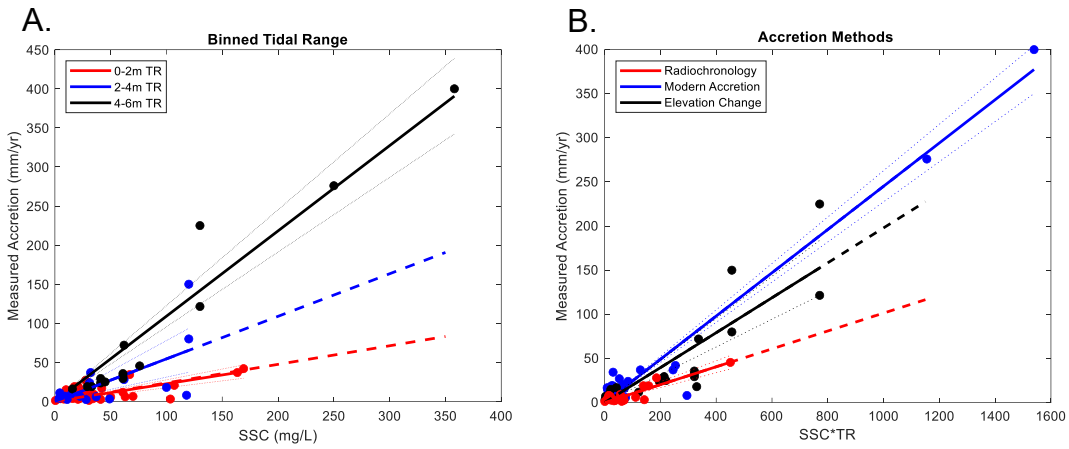


Figure 2: A. Measured accretion rate is linearly positively related to SSC for a given TR B. Relationship between accretion, SSC, and TR is dependent on methodology, with radiochronology (red) having a significantly lower slope than modern accretion (blue) or elevation change (black).

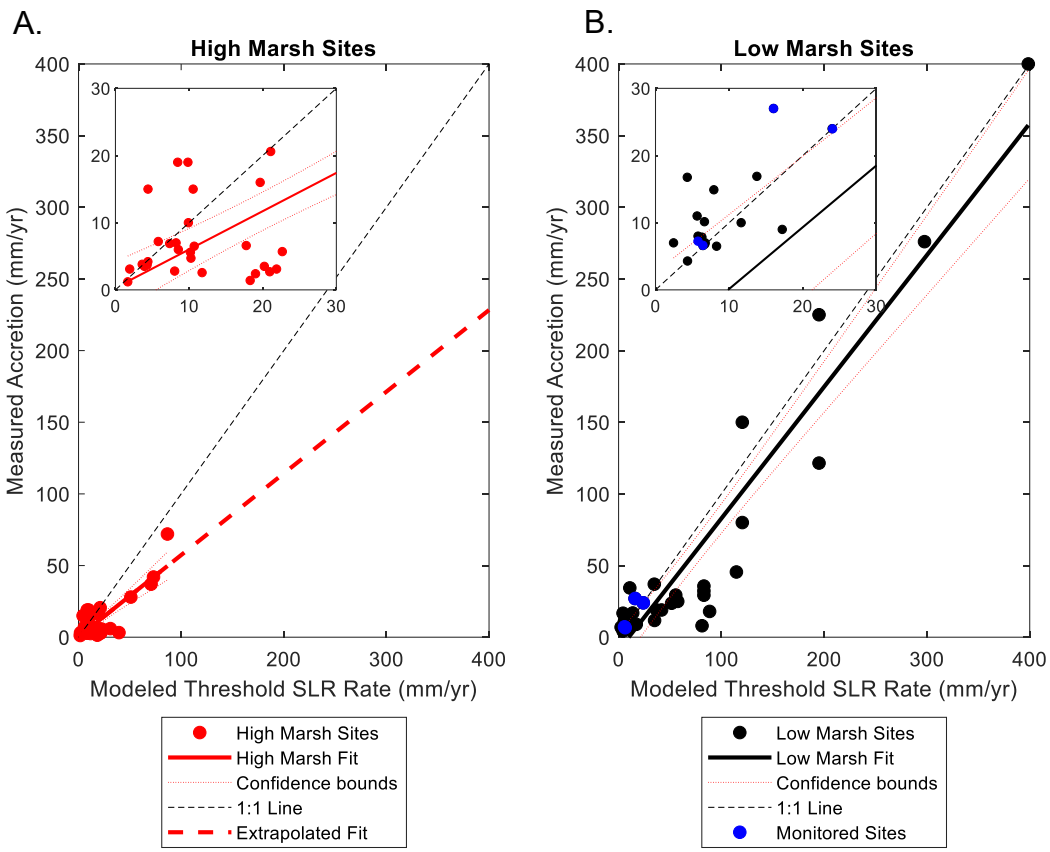


Figure 3: A. Comparison of observed accretion rate with threshold SLR determined from the ensemble model for high marsh sites. B. Comparison of observed accretion rate with threshold SLR determined from the ensemble model for only sites that were reported as low marsh. Blue points represent the four low marsh monitoring sites, and the insets are a magnified view of 0-30 mm $yr^{-1}$.

A.

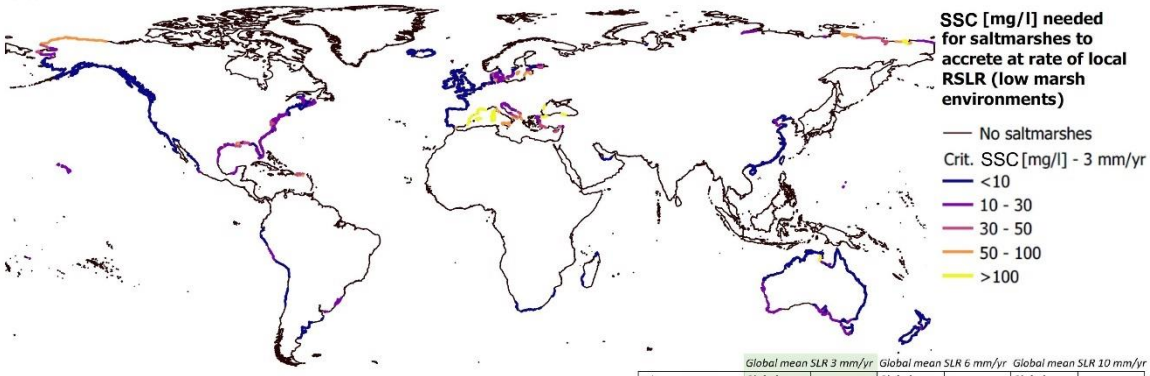


SSC crit = RSLR / (0.2250 x Spring Tidal Range)

| | | Global mean SLR 3 mm/yr | | Global mean SLR 6 mm/yr | | Global mean SLR 10 mm/yr | |
|---|---|---|---|---|---|---|---|
| Crit. SSC range [mg/l] | | Global area [km2] | Fraction [%] | Global area [km2] | Fraction [%] | Global area [km2] | Fraction [%] |
| 0 | 10 | 27,411 | 50 | 18,726 | 34 | 10,214 | 19 |
| 10 | 30 | 14,205 | 26 | 15,682 | 29 | 18,399 | 34 |
| 30 | 50 | 8,911 | 16 | 6,967 | 13 | 6,345 | 12 |
| 50 | 100 | 2,712 | 5 | 10,259 | 19 | 12,928 | 24 |
| 100 | 14533 | 1,424 | 3 | 3,028 | 6 | 6,775 | 12 |

B.

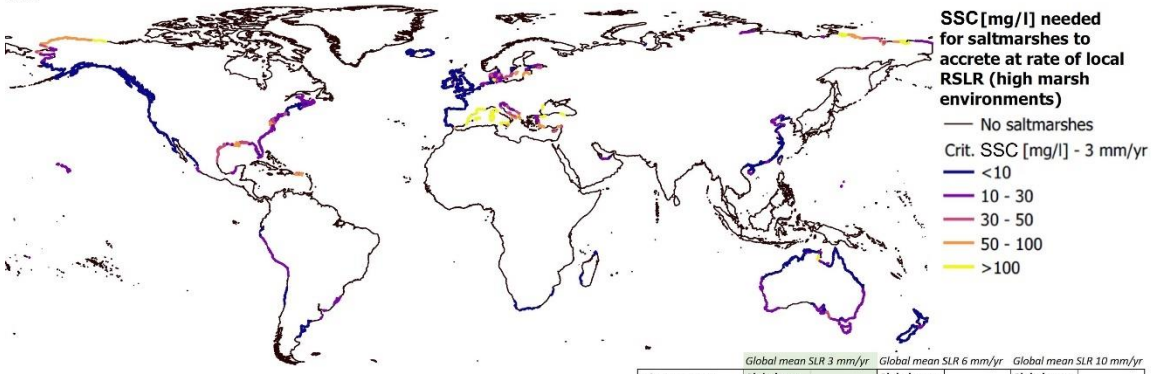


SSC crit = RSLR / (0.1624 x Spring Tidal Range)

| | | Global mean SLR 3 mm/yr | | Global mean SLR 6 mm/yr | | Global mean SLR 10 mm/yr | |
|---|---|---|---|---|---|---|---|
| Crit. SSC range [mg/l] | | Global area [km2] | Fraction [%] | Global area [km2] | Fraction [%] | Global area [km2] | Fraction [%] |
| 0 | 10 | 24,329 | 45 | 13,714 | 25 | 3,639 | 7 |
| 10 | 30 | 11,308 | 21 | 17,116 | 31 | 18,540 | 34 |
| 30 | 50 | 8,759 | 16 | 6,645 | 12 | 9,567 | 18 |
| 50 | 100 | 8,262 | 15 | 10,727 | 20 | 7,613 | 14 |
| 100 | 14533 | 1,981 | 4 | 6,459 | 12 | 15,292 | 28 |

Figure 4: A. World map indicating critical SSC needed for low marshes to maintain current elevation. B. SSC required for high marshes to maintain current elevation.

672 Supplementary Table 1: List of all sites included in the meta-analysis. Source refers to the original data source. All SSC are in mg $L^{-1}$, Accretion
673 rates (Acc.) are in mm $yr^{-1}$, and TR are spring tidal ranges in meters. Marsh or Channel and Sensor or Bottle columns refer to how SSC was
674 measured, with the letter corresponding to the first letter of the methodology. The Acc. Method column refers to how accretion rates were
675 measured and are classified as either radiochronology (R), modern accretion (A), or elevation change (E). If the site was specifically described as
676 a low elevation marsh, it is indicated with an X.
677

| *Location* | *SSC Source* | *SSC* | *Marsh or Channel* | *Sensor or Bottle* | *Accretion Source* | *Acc.* | *Acc. Method* | *Low Marsh* | *TR* |
|---|---|---|---|---|---|---|---|---|---|
| **Plum Island, MA** | This Study | 5.2 | M | S | This Study | 6.6 | R | X | 3.6 |
| **Upper Plum Island, MA** | This Study | 4.4 | M | S | This Study | 11.0 | A | X | 3.6 |
| **Goodwin Island, VA** | This Study | 13.4 | M | S | This Study | 7.2 | R | X | 1.1 |
| **Mockhorn Island, VA** | This Study | 27.6 | M | S | This Study | 27.0 | A | X | 1.9 |
| **South Altamaha, GA** | This Study | 31.0 | M | S | This Study | 24.0 | A | X | 2.7 |
| **North Altamaha, GA** | This Study | 22.4 | C | S | Loomis and Craft 2010 | 6.6 | R | | 2.7 |
| **Currambene Creek, Australia** | This Study | 0.5 | M | S | This Study | 1.2 | R | | 1.1 |
| **Scheldt Estuary** | Temmerman et al. 2004 | 130 | C | B | Temmerman et al. 2004 | 225 | E | X | 5.9 |
| **Scheldt Estuary** | Temmerman et al. 2004 | 109 | C | B | Temmerman et al. 2004 | 45.5 | R | X | 5.9 |
| **Scheldt Estuary** | Temmerman et al. 2004 | 76 | M | B | Temmerman et al. 2004 | 45.5 | R | X | 5.9 |
| **Scheldt Estuary** | Temmerman et al. 2004 | 41 | C | B | Temmerman et al. 2004 | 29.4 | E | X | 5.2 |
| **Scheldt Estuary** | Temmerman et al. 2004 | 33 | C | B | Temmerman et al. 2004 | 19 | R | X | 4.8 |
| **Scheldt Estuary** | Temmerman et al. 2004 | 29 | M | B | Temmerman et al. 2004 | 19 | R | X | 4.8 |
| **Scheldt Estuary** | Temmerman et al. 2004 | 41 | C | B | Temmerman et al. 2004 | 23.7 | E | X | 4.8 |
| **Scheldt Estuary** | Temmerman et al. 2004 | 61 | C | B | Temmerman et al. 2004 | 35.7 | E | X | 5.3 |
| **Scheldt Estuary** | Temmerman et al. 2004 | 61 | C | B | Temmerman et al. 2004 | 29.3 | E | X | 5.3 |

| | | | | | | | | | |
|---|---|---|---|---|---|---|---|---|---|
| **Scheldt Estuary** | Temmerman et al. 2004 | 61 | C | B | Temmerman et al. 2004 | 32.3 | E | X | 5.3 |
| **Scheldt Estuary** | Temmerman et al. 2004 | 104 | C | B | Temmerman et al. 2004 | 23.5 | R | X | 4.1 |
| **Scheldt Estuary** | Silinski et al. 2016 | 62 | C | B | Silinski et al. 2016 | 72 | E | | 5.4 |
| **Elbe Estuary** | Kappenberg & Grabeman 2001 | 120 | C | B | Schoutens et al. 2019 | 150 | E | X | 3.8 |
| **Elbe Estuary** | Kappenberg & Grabeman 2001 | 120 | C | B | Schoutens et al. 2019 | 80 | E | X | 3.8 |
| **Delaware Bay** | Stumpf 1983 | 5 | M | B | Kim et al. 1997 | 3.5 | R | | 1.8 |
| **Cedar Creek, FL** | Leonard et al. 1995 | 12.5 | M | B | Leonard et al. 1995 | 7.2 | A | | 1.2 |
| **Choptank River** | Ensign et al. 2014 | 17.5 | C | B | Ensign et al. 2014 | 19 | A | | 1.4 |
| **Choptank River** | Ensign et al. 2014 | 21 | C | S | Ensign et al. 2014 | 19 | A | | 1.4 |
| **Pocomoke River** | Ensign et al. 2014 | 10 | C | B | Ensign et al. 2014 | 15 | A | | 1 |
| **Pocomoke River** | Ensign et al. 2014 | 31 | C | B | Ensign et al. 2014 | 15 | A | | 1 |
| **Blackwater Wildlife Refuge, MD** | Stevenson et al. 1985 | 103.5 | C | B | Stevenson et al. 1985 | 3.1 | R | | 0.7 |
| **Hengsha Island, Yangzte** | Qing et al. 2003 | 250 | C | B | Yang et al. 2000 | 276 | A | X | 4.6 |
| **Town Creek, SC** | Murphy & Voulgaris 2006 | 28 | C | B | Sharma et al. 1987 | 2.4 | R | | 2.3 |
| **Oyster Landing, SC** | Murphy & Voulgaris 2006 | 30.5 | C | B | Sharma et al. 1987 | 1.4 | R | | 2 |
| **Mud Bay, North Inlet, SC** | Hutchinson et al. 1995 | 163.5 | C | B | Hutchinson et al. 1995 | 37 | A | | 1.5 |
| **Sixty Bass, North Inlet, SC** | Hutchinson et al. 1995 | 169.1 | C | B | Hutchinson et al. 1995 | 42 | A | | 1.5 |
| **Scheld Estuary** | Temmerman et al. 2004 | 130 | C | B | Vandenbruwaene et al., 2011 | 122 | E | X | 5.9 |
| **Scheld Estuary** | Wang & Temmerman, 2013 | 45 | C | B | Wang & Temmerman, 2013 | 25 | E | X | 4.9 |
| **Venice Lagoon** | Venier et al. 2014 | 20.7 | C | S | Bellucci et al. 2007 | 2.8 | R | | 1.1 |
| **Venice Lagoon** | Venier et al. 2014 | 29.1 | C | S | Day et al. 1999 | 6.5 | A | | 1.1 |
| **Venice Lagoon** | Carniello et al. 2012 | 16.6 | C | S | D'Alpaos et al. 2017 | 7 | R | X | 1.1 |
| **Wadden Sea, Dollart, Germany** | Ridderinkhof et al. 2000 | 100 | C | S | Esselink et al. 1998 | 18 | E | X | 3.3 |

| | | | | | | | | | |
|---|---|---|---|---|---|---|---|---|---|
| **Blythe Estuary, UK** | French et al. 2005 | 60.9 | C | S | French et al. 2005 | 11.7 | E | X | 2 |
| **Freemans Creek, NC** | Ensign & Currin, 2016 | 20.9 | M | B | Currin et al. 2017 | 10.2 | E | X | 0.8 |
| **Traps Bay Creek, New River, NC** | Ensign et al. 2017a | 16 | C | B | Currin et al. 2017 | 3.7 | E | | 0.6 |
| **French Creek, New River, NC** | Ensign et al. 2017a | 8 | C | B | Currin et al. 2017 | 3.1 | E | | 0.2 |
| **Nelson Island, Plum Island, MA** | LeMay 2007 | 9.3 | C | B | Kirwan et al. 2011 | 2 | R | | 3.6 |
| **Club Head Creek, Plum Island, MA** | LeMay 2007 | 11 | C | B | Kirwan et al. 2011 | 2.6 | R | | 3.6 |
| **Blackwater Wildlife Refuge, MD** | Ganju et al. 2017 | 63 | C | S | Ganju et al. 2015 | 6 | A | | 0.4 |
| **Fishing Bay, MD** | Ganju et al. 2017 | 39 | C | S | Ganju et al. 2015 | 4.7 | A | | 0.8 |
| **Ogunquit, ME** | Ganju et al. 2017 | 3.7 | C | S | Neil Ganju | 3.8 | E | | 2.1 |
| **Seal Beach, CA** | Ganju et al. 2017 | 15 | C | S | Rosencranz et al. 2017 | 10 | A | X | 2.5 |
| **Point Mugu, CA** | Ganju et al. 2017 | 15 | C | S | Rosencranz et al. 2017 | 7 | A | | 1.6 |
| **Reedy Creek, NJ** | Ganju et al. 2017 | 9.5 | C | S | Elsey-Quirk 2016 | 7 | E | X | 0.3 |
| **Potomac River** | Palinkas & Engelhardt 2018 | 22.1 | C | B | Palinkas & Engelhardt 2018 | 6.9 | A | | 0.9 |
| **Bayou Chitigue, LA** | Wang 1997 | 20 | C | B | Cahoon et al. 2006 | 16.8 | A | X | 0.4 |
| **Bayou Chitigue, LA** | Day et al. 2011 | 67 | C | B | Day et al. 2011 | 34.4 | A | X | 0.4 |
| **Old Oyster Bayou, LA** | Day et al. 2011 | 107 | C | B | Day et al. 2011 | 20.6 | A | X | 0.6 |
| **St. Jones, DE** | Moskalski & Sommerfield, 2012 | 6 | M | B | Kraft et al. 1992 | 4.3 | R | X | 1.7 |
| **Bombay Hook, DE** | Sommerfield & Wong, 2011 | 9 | C | S | Kraft et al. 1992 | 6.8 | R | X | 2.1 |
| **Bayou Penchant, LA** | Lane et al. 2002 | 26.2 | C | B | DeLaune et al. 1987 | 7.8 | R | X | 0.6 |
| **Fourleague Bay, LA** | Lane et al. 2002 | 70 | C | B | DeLaune et al. 1987 | 6.5 | R | X | 0.3 |
| **Napa River, CA** | Buchanan & Ganju, 2003 | 49 | C | S | Schile et al. 2014 | 3.2 | R | | 2.9 |
| **Mallard Island, CA** | Buchanan & Ganju, 2003 | 41 | C | S | Schile et al. 2014 | 2.7 | R | | 1.7 |

| | | | | | | | | | |
|---|---|---|---|---|---|---|---|---|---|
| **San Mateo Bridge, CA** | Buchanan & Ganju, 2003 | 37 | C | S | Patrick & Delaune, 1990 | 6 | R | | 3 |
| **Far South SF Bay, CA** | Buchanan & Ganju, 2003 | 62 | C | S | Watson 2004 | 28 | R | | 3 |
| **Tagus Estuary, Portual** | Vale & Sundby, 1987 | 32 | C | B | Salgueiro & Cacador 2007 | 37 | A | X | 4 |
| **Skallingen, Denmark** | Bartholdy & Anthony 1998 | 35 | C | S | Bartholdy & Madsen 1985 | 9 | R | X | 1.6 |
| **Sylt, Wadden Sea, Germany** | Scheurch et al. 2013 | 34 | M | B | Scheurch et al. 2012 | 3.5 | R | | 2 |
| **Wax Lake Delta, LA** | W. Wagner, unpublished | 22 | C | S | Wagner et al. 2017 | 14.9 | E | X | 1 |
| **Wax Lake Delta, LA** | W. Wagner, unpublished | 42 | C | S | Wagner et al. 2017 | 16.9 | E | X | 1 |
| **Dyfi Estuary, Wales** | S. Jackson, unpublished | 15.7 | C | B | Shi 1993 | 16.0 | A | | 4.5 |
| **Delaware Bay Mouth** | Haaf et al. 2019 | 50 | C | B | Haaf et al. 2019 | 5.7 | A | | 1.5 |
| **Delaware River** | Haaf et al. 2019 | 16 | C | B | Haaf et al. 2019 | 10.0 | A | | 1.9 |
| **Barnegut Bay, NJ** | Haaf et al. 2019 | 23 | C | B | Haaf et al. 2019 | 4.2 | A | | 0.4 |
| **San Pablo Bay, CA** | Lacy et al. 2019 | 118 | M | S | Lacy et al. 2019 | 8.0 | A | X | 2.5 |
| **Yinshuichuan, Yangtze, China** | Chen et al. 2003 | 358 | C | B | Yang et al. 2003 | 400 | A | X | 4.3 |
| **Suncheon Bay, South Korea** | Lee et al. 2008 | 312 | C | B | Lee et al. 2008 | 55 | A | X | 3.1 |
| **Allen Creek, Canada** | Davidson-Arnott et al. 2002 | 117 | M | S | van Proosdij et al., 2006 | 14 | E | | 12 |
| **Kingsport, Canada** | Proirier et al. 2017 | 53 | M | S | Proirier et al. 2017 | 11.4 | A | | 11 |

678

679 Supplementary Table 2: Additional details on the four low marsh monitoring sites.
680

| Location | Site Affiliation | S. alterniflora form | Latitude | Longitude | Monitoring Duration | Accretion Verification |
|---|---|---|---|---|---|---|
| **Plum Island, MA** | PIE LTER | Short | 42°43'55.43"N | 70°50'30.78"W | 9 months | Comparison to Wilson et al. 2014 |
| **Goodwin Island, VA** | CB NERR | Tall | 37°13'15.35"N | 76°24'56.29"W | 24 months | Aerial imagery and core properties |
| **Mockhorn Island, VA** | VCR LTER | Tall | 37°16'51.35"N | 75°52'44.83"W | 18 months | Aerial imagery and core properties |
| **South Altamaha, GA** | GCE LTER | Tall | 31°18'10.07"N | 81°24'22.52"W | 12 months | Aerial imagery and core properties |

Supplementary Table 3: The three predictive empirical models used to calculate accretion are given with corresponding constants. The statistical measures are based on a linear regression between measured accretion and accretion predicted using the empirical model.

| ***Model Type*** | ***Equation*** | ***Fitted Coefficients*** | ***RMSE*** | ***$R^2$*** | ***p-value*** |
|---|---|---|---|---|---|
| *1. Simplest* | $A = C_1 * SSC * TR$ | $C_1$=0.22 | 21.3 | 0.89 | <0.001 |
| *2. Logistic* | $A = \left(\frac{C_1 - C_2}{1 + e^{C_3(TR - C_4)}} + C_2\right) * SSC$ | $C_1$=1.10, $C_2$=0.18, $C_3$=-3.45, $C_4$=3.13 | 18.7 | 0.91 | <0.001 |
| *3. Best Fit Linear* | $A = C_1 * SSC + C_2 * TR + C_3 * SSC * TR$ | $C_1$=-0.27, $C_2$=-10.1, $C_3$=0.32 | 18.1 | 0.92 | <0.001 |

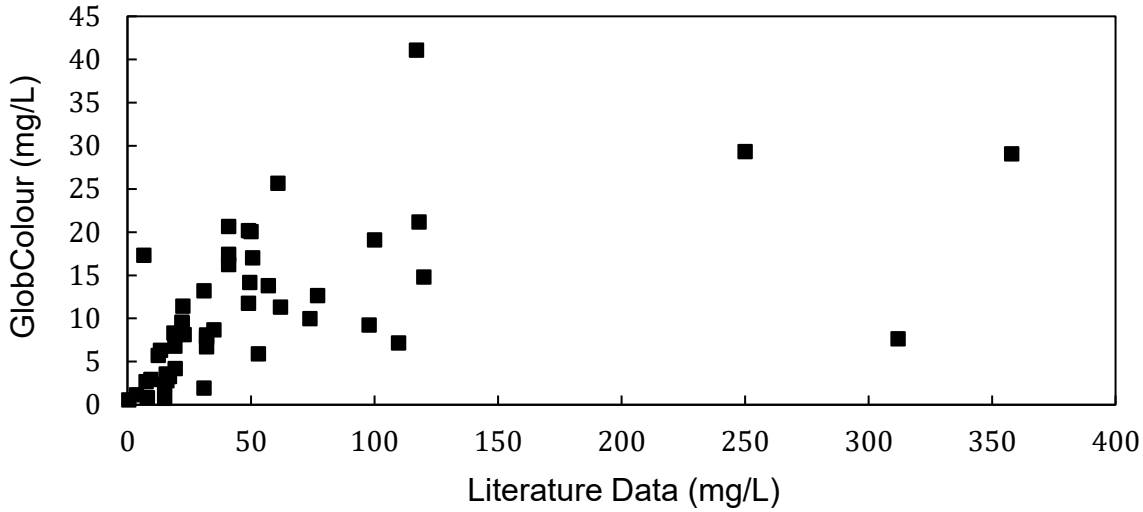


Supplementary Figure 1: Comparison of GlobColour satellite-derived SSC and literature-derived field measurements.

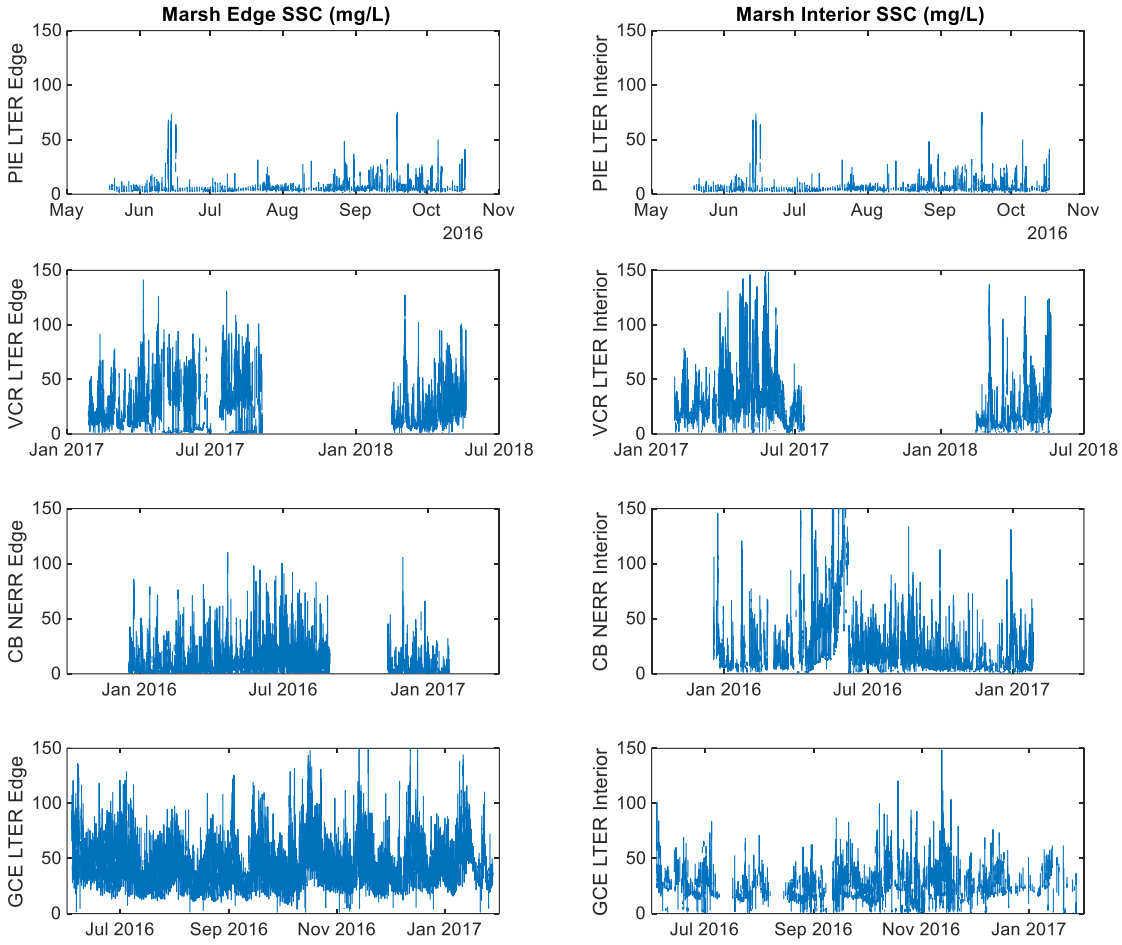


Supplementary Figure 2: SSC time series of the marsh edge and interior of the four low marsh sites. Note differences in the x-axis that correspond to different monitoring lengths. Gaps in the record represent times when the sensors were being repaired or field conditions prohibited site monitoring.

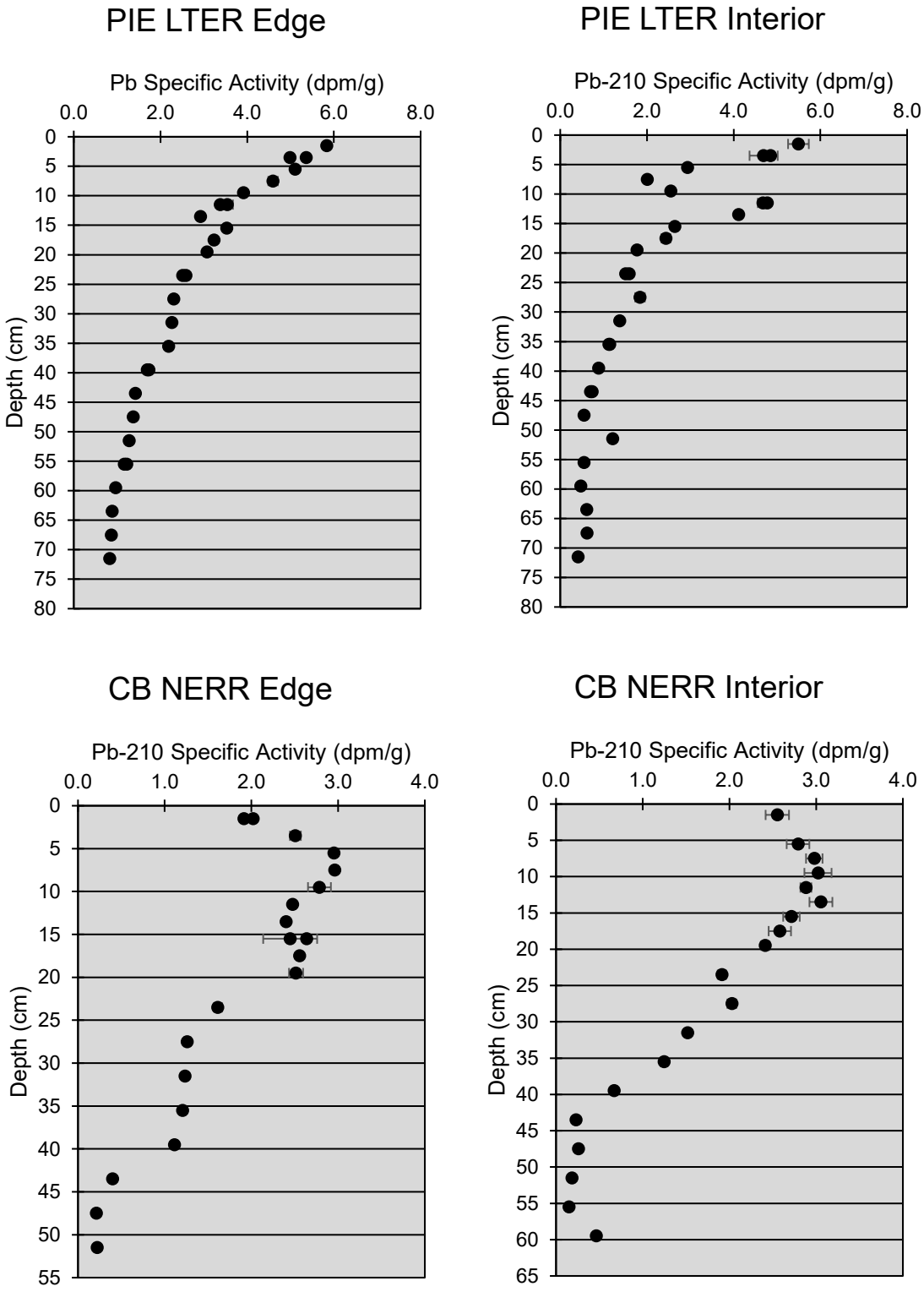
PIE LTER Edge
Pb Specific Activity (dpm/g)
0.0
2.0
4.0
6.0
8.0
Depth (cm)
0
5
10
15
20
25
30
35
40
45
50
55
60
65
70
75
80
PIE LTER Interior
Pb-210 Specific Activity (dpm/g)
0.0
2.0
4.0
6.0
8.0
Depth (cm)
0
5
10
15
20
25
30
35
40
45
50
55
60
65
70
75
80
CB NERR Edge
Pb-210 Specific Activity (dpm/g)
0.0
1.0
2.0
3.0
4.0
Depth (cm)
0
5
10
15
20
25
30
35
40
45
50
55
CB NERR Interior
Pb-210 Specific Activity (dpm/g)
0.0
1.0
2.0
3.0
4.0
Depth (cm)
0
5
10
15
20
25
30
35
40
45
50
55
60
65

693

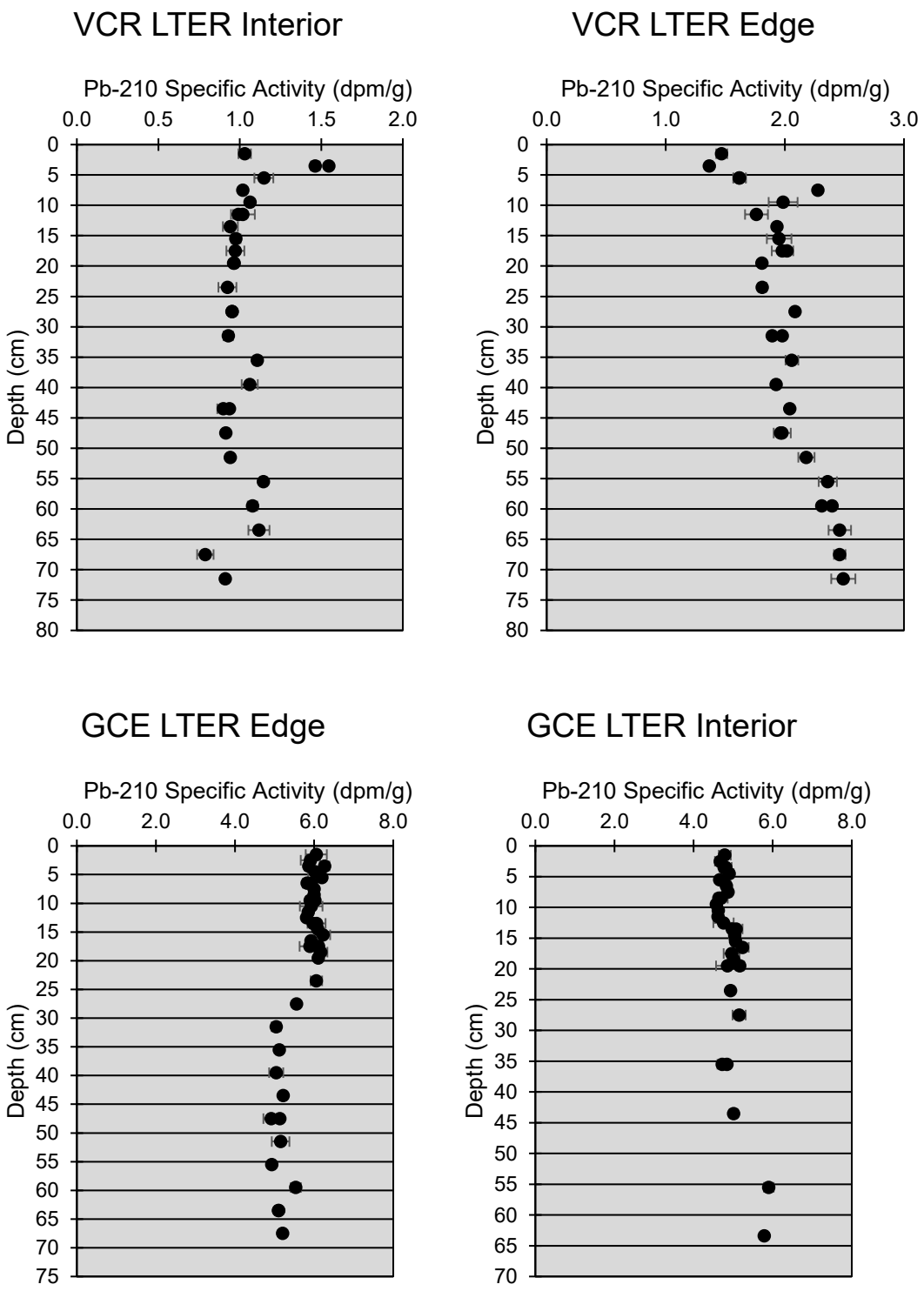


Supplementary Figure 3: Pb-210 total activity in sediment cores from the edge and interior of the four low marsh sites. Accretion rates of 6.6 mm $yr^{-1}$ and 7.2 mm $yr^{-1}$ were calculated for PIE LTER and CB NERR sites, respectively, whereas no accretion rate could be calculated for GCE LTER or VCR LTER.

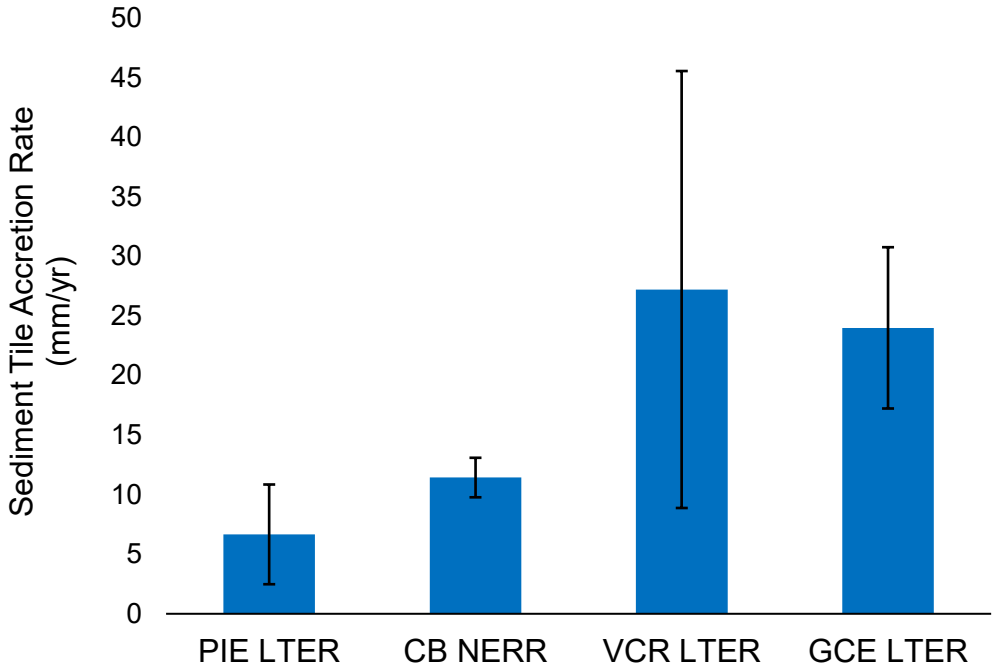


Supplementary Figure 4: Vertical marsh accretion rate measured on top of sediment tiles and/or grids. Error bars represent one standard deviation. The rates shown for the VCR LTER and GCE LTER were used in lieu of radiochronological rates.

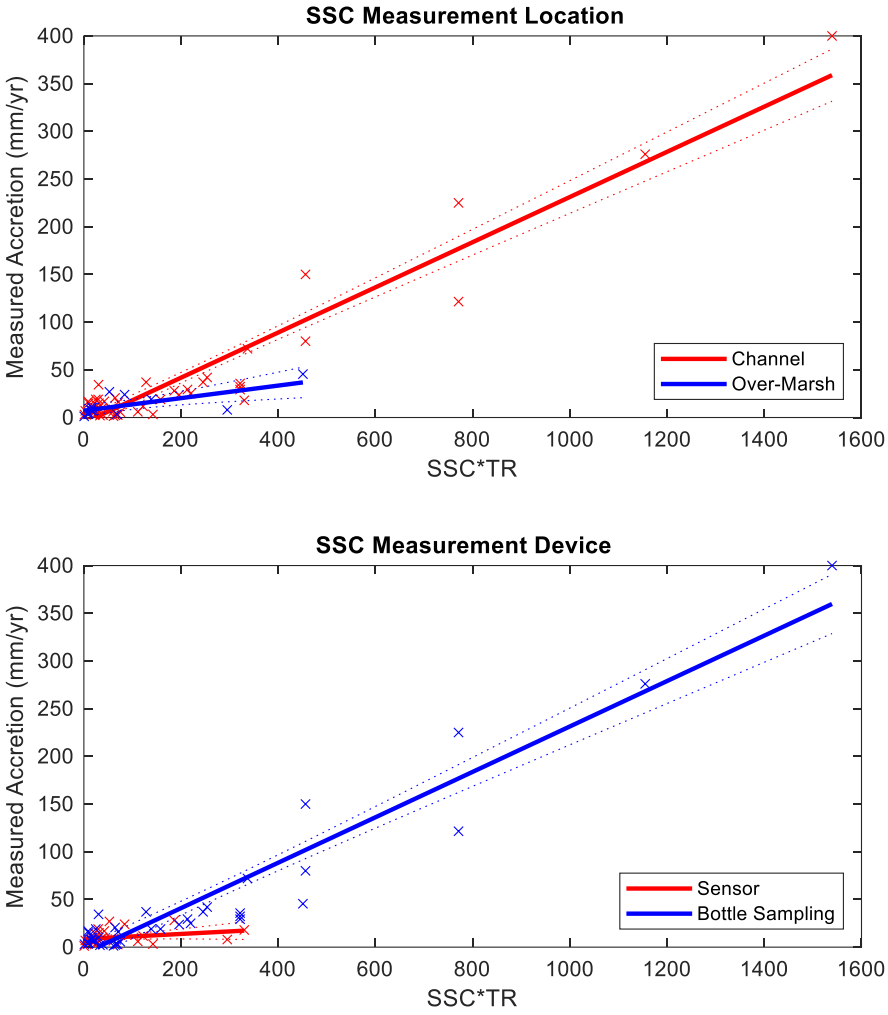


706
707 Supplementary Figure 5: Comparison of different SSC measurement methods. Note that channel
708 sampling and bottle sampling are the dominant approaches.